NAS Technical Report;
NAS-05-019
December 2005

36th AIAA Plasmadynamcis and Lasers Conference, 6-9 June 2005, Toronto, Ontario, Canada

A Numerical Study of Resistivity and Hall Effects for a Compressible MHD Model

B. Sjögreen * H. C. Yee †

The effect of resistive, Hall, and viscous terms on the flow structure compared with compressible ideal MHD is studied numerically for a one-fluid non-ideal MHD model. The goal of the present study is to shed some light on the emerging area of non-ideal MHD modeling and simulation. Numerical experiments are performed on a hypersonic blunt body flow with future application to plasma aerodynamics flow control in reentry vehicles. Numerical experiments are also performed on a magnetized time-developing mixing layer with possible application to magnetic/turbulence mixing.

I. Motivation

The role various components of the generalized Ohm's law can play in many of the physical phenomena encountered in physics and engineering is not fully understood. Four of the emerging areas of non-ideal MHD modeling are: (a) Plasma aerodynamic flow control for possible drag reduction, normal force control and heat transfer minimization of highly maneuverable high speed combat aircraft and reentry vehicles, (b) Reentry vehicles at hypersonic speed that develop ionized plasma that creates a magnetic field which can affect the design of heat shield, flight control and communication apparatus, (c) Plasma detachment or magnetic reconnection (MR) in the design of Tokamak reactors, in plasma rocket exhaust and in the dynamics of solar coronal mass ejections and their effect on the structure of the solar wind, the heliospheric magnetic field and planetary magnetospheres,[1,4] and (d) Laser, fusion and high energy density physics.

Pertaining to areas (a) and (b), for example, in hypersonic blunt body gas dynamics flow, it is known that different equations of state and evolutionary equation sets (e.g., non-equilibrium flows) can affect the shock standoff distance and bow shock shape, and consequently heating of the blunt body. Plasma injection in hypersonic reentry vehicles for possible heat transfer minimization is important in the design of heat shield of the vehicle. Pertaining to areas (c) and (d), aside from dealing with general equations of state, multi-fluid and multi-phase flows, for some MHD modeling, in order for plasma detachment or MR to proceed, there must be some mechanism which can violate the ideal MHD condition in the diffusion region and allow plasma to diffuse across the magnetic field. One of the candidates for breaking the ideal MHD condition is resistivity.[6,11] Another candidate is the well known Hall effect and thermal inertia terms.[7,8] A third candidate is through turbulent reconnection and reconnection in chaotic magnetic fields.[2,9]

In order to shed some light on the effect of the resistive and Hall coefficients on the flow structure, we first perform numerical study on a one-fluid non-ideal MHD model. Numerical experiments on (a) a Mach 15 and 2.60 blunt body flow and (b) a magnetized version of a vortex pairing in the time-developing mixing layer problem that was previously investigated by the authors and collaborators[17] are conducted. For the blunt body problem the effect of the resistive and Hall coefficients on the shock standoff distance

*NADA, KTH, Stockholm, Sweden
†NASA Ames Research Center, Moffett Field, CA, USA

and bow shock shape compared with the perfect gas and ideal MHD cases will be illustrated. The effect of the structure of the bow shock as a function of the plasma β (β_p) will also be investigated. Due to the simple flow structure of the blunt body problem, only second-order shock-capturing methods are used for the simulation. The magnetized version of a vortex pairing in the time-developing mixing layer problem is a time-accurate computation with complex flow structure. Our adaptive numerical dissipation control in high order filter schemes[12,13,17,18,20–22] is used for the simulation. It was shown that our scheme is stable and accurate for a wide spectrum of flow physics ranging from long time wave propagation of smooth flows to high speed multiscale turbulent flows including strong shock waves. Two unique features of our scheme are (a) Solving the ideal conservative MHD system (a non-strictly hyperbolic system of conservation laws) without having to deal with its incomplete eigensystem, and (b) Adaptive numerical dissipation control that permits, at ease, the minimization of the divergence of the magnetic field ($\nabla\cdot\mathbf{B}$) numerical error. Since second-order shock-capturing schemes are well known and can be found in many text books and review articles,[16] the next section gives only a brief review of our high order filter scheme. Numerical experiments on the one-fluid resistive MHD model will be given in Section III.

II. Designing Adaptive Low Dissipative High Order Schemes for the Compressible MHD Equations

Our adaptive numerical dissipation control in high order filter schemes[12,18] consists of automatic detection of different flow features by distinct sensors to signal the appropriate type and amount of numerical dissipation/filter where needed while leaving the rest of the region free of numerical dissipation contamination. These scheme-independent detectors are capable of distinguishing shocks/shears, flame sheets, turbulent fluctuations and spurious high-frequency oscillations. In addition, these sensors are readily available as an improvement over existing grid adaptation indicators. The detection algorithm is based on an artificial compression method (ACM) (for shocks/shears), and redundant multiresolution wavelets (WAV) (for all types of flow feature). The ACM and wavelet filter schemes with sixth-order spatial central scheme for both the inviscid and viscous flux derivatives and a fourth-order Runge-Kutta method (RK4) are denoted by ACM66 and WAV66. A second-order MUSCL spatial scheme with a second-order Runge-Kutta method (RK2) is denoted by (MUSCL).

In our previous work, extensive grid convergence studies were performed using WAV66 and ACM66 for many well tested model problems. In many instances, grid convergence was achieved by ACM66 and WAV66 but not by MUSCL using the same grid sequence. More accurate solutions were obtained with WAV66 and ACM66 than with MUSCL, which requires similar CPU time, and a fifth order weighted ENO scheme (WENO5-RK4), which is nearly three times as expensive. See[12,13,17,18,20–23] for details. The following subsections give an brief overview of features (a) and (b) and a description of the filter method.

A. Solving Conservative MHD Systems Using Symmetrizable Eigenvectors

Consider the 3-D conservative and symmetrizable[5] (non-conservative) forms of the ideal compressible MHD equations,

$$U_t + \nabla\cdot\mathbf{F} = 0 \quad \text{(conservative)}, \tag{1}$$

$$U_t + \nabla\cdot\mathbf{F} = S \quad \text{(symmetrizable)}, \tag{2}$$

$$U = \begin{pmatrix} \rho \\ \rho u \\ \rho v \\ \rho w \\ e \\ B_x \\ B_y \\ B_z \end{pmatrix} ; \mathbf{F} = \begin{pmatrix} \rho \mathbf{u} \\ \rho \mathbf{u}\mathbf{u}^T + (p + B^2/2)I - \mathbf{B}\mathbf{B}^T \\ \mathbf{u}(e + p + B^2/2) - \mathbf{B}(\mathbf{u}^T\mathbf{B}) \\ \mathbf{u}\mathbf{B}^T - \mathbf{B}\mathbf{u}^T \end{pmatrix} ; S = -(\nabla \cdot \mathbf{B}) \begin{pmatrix} 0 \\ B_x \\ B_y \\ B_z \\ \mathbf{u}^T\mathbf{B} \\ u \\ v \\ w \end{pmatrix}. \quad (3)$$

The velocity vector $\mathbf{u} = (u, v, w)^T$, the magnetic field vector $\mathbf{B} = (B_x, B_y, B_z)^T$, ρ is the density, and e is the total energy. The notation $B^2 = B_x^2 + B_y^2 + B_z^2$ is used. The pressure is related to the other variables by

$$p = (\gamma - 1)(e - \frac{1}{2}\rho(u^2 + v^2 + w^2) - \frac{1}{2}(B_x^2 + B_y^2 + B_z^2)).$$

For plasmas and monatomic gases, $\gamma = 5/3$. The vector on the right hand side of (2) is the non-conservative portion of the symmetrizable MHD equations and is frequently referred to in the literature as a source term vector. The conservative and symmetrizable forms of the non-ideal compressible MHD[3] (viscous, resistive and Hall MHD) take the form

$$U_t + \nabla \cdot \mathbf{F} = \mathbf{F}_v,$$

$$U_t + \nabla \cdot \mathbf{F} = \mathbf{F}_v + S,$$

$$\mathbf{F}_v = [\ 0 \quad \mathrm{div}\tau \quad f_{v5} \quad \frac{1}{\sigma}(\triangle\mathbf{B} - \nabla \mathrm{div}\mathbf{B}) - \beta_h \nabla \times ((\nabla \times \mathbf{B}) \times \mathbf{B})\ ]^T.$$

The fifth component of $\mathbf{F}_v$ is

$$f_{v5} = \mathrm{div}(\mathbf{u}^T\tau) + \mathrm{div}\mathbf{h} - \frac{1}{\sigma}\mathrm{div}((\nabla \times \mathbf{B}) \times \mathbf{B}) - \beta_h \mathrm{div}\left(((\nabla \times \mathbf{B}) \times \mathbf{B}) \times \mathbf{B}\right).$$

The vector $\mathbf{F}_v$ includes viscosity, resistivity, and Hall effect with τ being the viscous stress tensor, σ the conductivity coefficient, β_h the strength of the Hall effect (β with subscript "h"), and $\mathbf{h}$ the heat flux. The notation for the plasma β (β with subscript "p") β_p = (plasma pressure/magnetic pressure) will be used.

An important ingredient in our high order filter method is the use of the dissipative portion of high-resolution shock-capturing schemes as part of the nonlinear filters for discontinuity capturing. These nonlinear filters usually involve the use of approximate Riemann solvers (knowledge of the eigenstructure of the system). Due to the fact that the conservative MHD system (1) is a non-strictly hyperbolic conservation law, we proposed in[13,21] to solve (1) using the eigenvectors of the symmetrizable system (2). See[13,21] for details.

B. Divergence-Free Preserving High Order Filter Methods

The filter method consists of two steps, a divergence-free preserving (base scheme) step (not involving the use of approximate Riemann solvers or flux limiters) and a filter step (usually involving the use of approximate Riemann solvers and flux limiters). The type of base schemes is very general. The adaptive filter is scheme independent and can be used in conjunction with spectral, compact or non-compact spatially central base schemes. In order to have good shock-capturing capability, improved nonlinear stability related to spurious high frequency oscillations, and no interference with the accuracy of turbulent fluctuation, the blending of a high order nonlinear filter and a high order linear filter was proposed by Yee & Sjögreen.[18,21] The nonlinear filter consists of the **product** of an ACM or wavelet flow sensor and the nonlinear dissipative portion of a high-resolution shock-capturing scheme. The high order linear filter consists of the product of another

sensor, a tuning parameter and a high order centered linear dissipative operator that is compatible with the order of the base scheme being used. Three forms of the nonlinear dissipative portion of shock-capturing are considered, namely:

- Dissipative portion of the fifth-order WENO scheme (WENO5). It can be obtained, e.g., in the x-direction by taking the full WENO5 scheme in the x-direction and subtracting (a) $D_{06}F_j$ (sixth-order central differencing) or $D_{04}F_j$ (fourth-order central differencing).
- Dissipative portion of the a second-order MUSCL scheme.[17]
- Dissipative portion of the Harten-Yee TVD scheme.[17,21]

The resolution of the above forms of the dissipative portion of shock-capturing schemes are comparable and work well on all of our numerical tests for both the ideal and resistive viscous MHD systems. See Yee & Sjögreen[22] and references cited therein for details.

The nonlinear filter we proposed, if applied to the entire MHD system, will not preserve the divergence free magnetic field condition in general. For the computations in this paper, the "**No filter on B**" option is chosen. That is, the nonlinear filter step only applies to the first five equations of (1) or (2). With the divergence free spatial base scheme, the divergence free property should be preserved for periodic boundary conditions on uniform Cartesian grids. Extensive grid convergence comparison of the "no filter on **B**" with the "filter all of the MHD equations" options were presented in.[20,21] Extension of these schemes to curvilinear grids is straightforward.[15] Non-staggered divergence cleanings (central differencing) can be used in the non-uniform grid case.

III. Numerical Experiment

For the numerical experiment, we chose (a) a Mach 15 blunt body and the De Sterck and Poedts[14] (Mach 2.60, $\beta_p = 0.4$) blunt body flows, and (b) a magnetized version of a vortex pairing in time-developing mixing layer problem that was previously investigated by the authors and collaborators.[12,17,18] The Mach number is defined as the ratio between the free stream velocity and the sound speed, $c = \sqrt{\gamma p/\rho}$. The value of the magnetic Mach number, $M_A = 1.5$, in[14] corresponds to $M = 2.60$ for the Mach number defined by the sound speed. In the computations the variables are normalized such that the free stream state is $\rho_\infty = 1$, $u_\infty = M\sqrt{\gamma p_\infty}$, $B_\infty = \sqrt{2p_\infty/\beta_p}$. The free stream pressure is $p_\infty = 1$ for the Mach 15 case, and $p_\infty = 0.2$ for the Mach 2.60 case.

Blunt Body Results ($\mathbf{M = 15}$ & $\mathbf{2.60}$): For this problem, only second-order shock-capturing schemes using a second-order Runge-Kutta temporal discretization (RK2) solving the symmetrizable MHD system (2) are employed for the study. For time-marching to the steady states, the schemes have problems with convergence if we solve the conservative MHD system (1). The reason is not certain and is currently under investigation.

Figure 1 shows the comparison among perfect gas, ideal MHD with two plasma β ($\beta_p = 5, 10$), resistive MHD with $Re = 1000, \sigma = 100, \beta_p = 5$, and Hall MHD with the Hall coefficient $\beta_h = 0.5$. The computation shown uses a second-order MUSCL scheme with the van Albada limiter using a mildly stretched parabolic curvilinear 121×41 grid. Grid refinement on the perfect gas and ideal MHD cases indicate that the 121×41 grid is sufficient to obtain an accurate solution. The shock standoff distance and the bow shock shape are very different among the perfect gas, ideal MHD and resistive MHD. For the non-ideal MHD cases, finer grids improve the resolution near the wall.

For the Hall coefficient $\beta_h \leq 0.5$, the Hall effect is very small compared with the resistive MHD for the same $Re = 1000$, $\sigma = 100$ and plasma β_p in the range $(0.15, 10)$. As the Hall coefficient β_h increases,

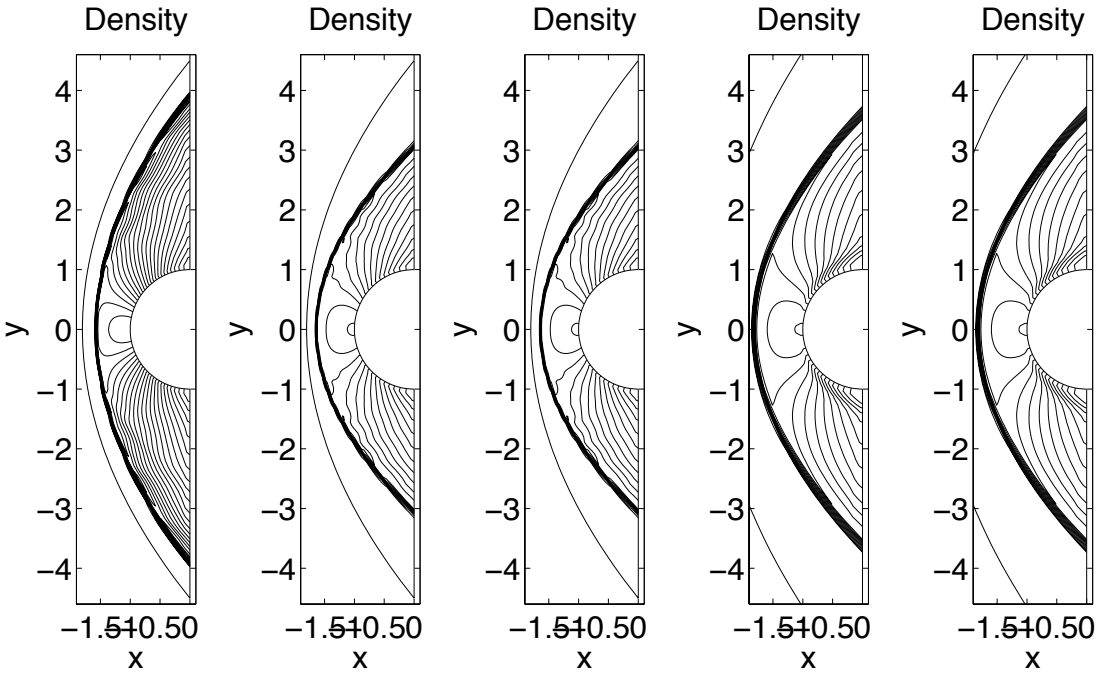

Fig. 1 Blunt body problem with $M = 15$. Density contours comparison by second-order MUSCL with an 121×41 grid (left to right): Perfect Gas, Ideal MHD $\beta_p = 5$, Ideal MHD $\beta_p = 10$, Resistive MHD $Re = 1000, \sigma = 100, \beta_p = 5, \beta_h = 0$, Hall MHD $Re = 1000, \sigma = 100, \beta_p = 5, \beta_h = 0.5$.

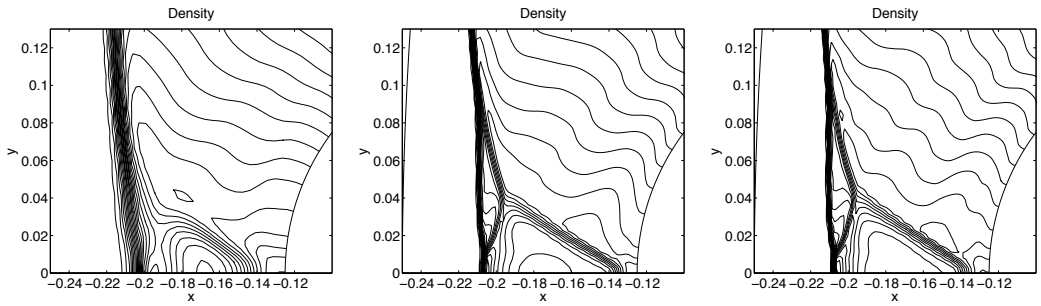

Fig. 2 Blunt body problem with $M = 2.60, \beta_p = 0.4$. Density contours comparison: Second-order Lax-Friedrichs, Harten-Yee and MUSCL using a 81×81 grid.

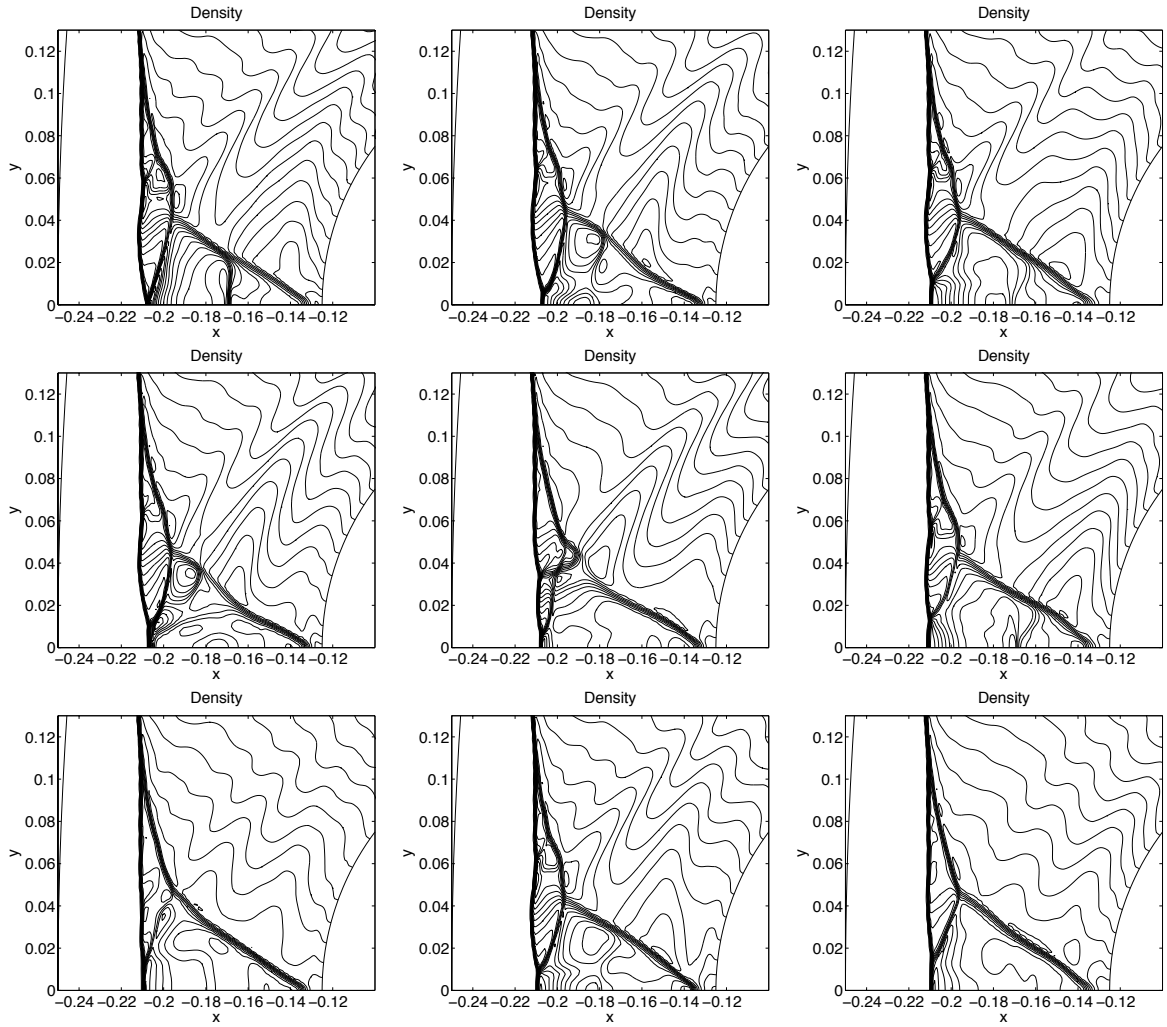

Fig. 3 Blunt body problem $M = 2.60, \beta_p = 0.4$. Density contours of the unsteady evolution on an 161×161 grid using MUSCL at 9 different time instances: T=80, 120, 160, 200, 560, 900, 1300, 1600, 2000.

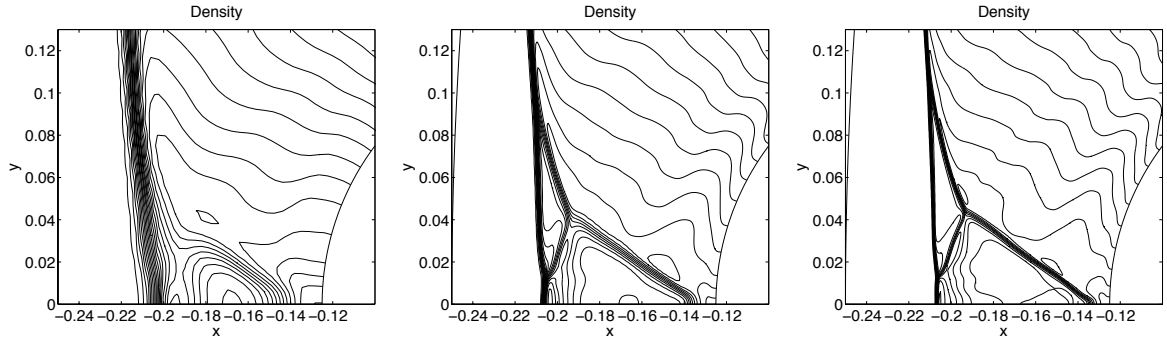

Fig. 4 Blunt body problem with $M = 2.60, \beta_p = 0.4$. Comparison: Density contours of the steady solutions by the second-order Lax-Friedrichs using 81×81, 161×161 and 321×321 grids.

the problem becomes very stiff and the scheme experiences convergence problems. Future study using the implicit stiffly stable local time-stepping approach is planned to further investigate the large β_h issue.

For the ideal MHD with large plasma β_p in the range of $(0.15, 10)$ there is no noticeable change in the shock standoff distance and bow shock shape. For $\beta_p \leq 1$, the bow shock standoff distance and bow shock shape change (figures not shown).

In the supersonic and low hypersonic range, the bow shock shape is more sensitive to the same range of β_p than the higher Mach number case (e.g., $M = 15$). To illustrate this point, we simulate the same problem as in De Sterck and Poedts.[14] For $M = 2.60$ and β_p below 0.7, DeSterck-Poedts concluded that intermediate shocks would developed using the second-order Lax-Friedrichs scheme with an 81×81 coarse grid. Their numerical solutions deviate from the standard bow shock shape near the stagnation region. See[10] for an overview of stability of intermediate shocks in conjunction with out of plane perturbations.

We perform an extensive grid refinement study (41×41 to 1281×1281 grids) on the De Sterck and Poedts blunt body problem for $M = 2.60$ and $\beta_p = 0.4$ in both time-accurate and time-marching to the steady state approaches. Figures 2-4 show some of the computations. As the grid is refined (larger than 101×101) using both time-accurate and time-marching approaches with CFL in the range of $(0.1, 0.8)$, there is no conclusive evidence that these intermediate shocks will settle down to a definite steady solution, a limit cycle or a spurious solution (numerical artifact).[19] For an 81×81 grid, the second-order Lax-Friedrichs, Harten-Yee and MUSCL all converge to the same steady state (time-accurate or time-marching simulations). As we refine the grid, Harten-Yee and MUSCL no longer converge to the same steady state solution, but rather have different (yet similar global pattern) and very complex irregular structure in the vicinity of the stagnation region (figures not shown). Figure 3 shows the time-accurate computation by MUSCL with an 161×161 grid (similar unsteady behavior for Harten-Yee). We simulate the problem with time-marching mode with the same grid, the numerical solution does not settle down but yields similar flow structures for MUSCL and Harten-Yee. This is not the case with second-order Lax-Friedrichs. Figure 4 shows the time-accurate computation by the second-order Lax-Friedrichs using three grids. All the solutions converge to the same steady state. The time-marching approach using the second-order Lax-Friedrichs also converges to the same steady state with the same grid. For a fine grid such as 641×641 or larger, even the diffusive Lax-Friedrichs scheme does not settle down to the same asymptote (using very large number of iterations). Without further research, our preliminary conclusion is that we cannot conclude if the asymptoes are stable.

Vortex Pairing in Time-Developing Mixing Layer Result: Figure 5 shows the schematic of the flow condition of the gas dynamics model studies in.[17] For the magnetized case, in addition to the gas dynamics initial conditions (ICs) and boundary conditions (BCs) indicated in Fig. 5, the initial magnetic field is 0.1 in the x-direction and zero in the other two directions. A grid mildly stretched in the y-direction and uniform in the x-direction is used. In Yee and Sjögreen,[23] a study of the resistive effect on the same one-fluid MHD model (1) and (2) without the Hall term was performed on this vortex pairing problem. To aid the discussion, we include the result from that study here.

Figure 6 shows the comparison of our ACM66-RK4 scheme with MUSCL-RK2. ACM66 required at least 50% fewer grid points per direction with similar resolution as MUSCL and WENO5-RK4 (figures not shown). Figure 7 shows the comparison of ideal MHD with viscous resistive MHD for $Re = 10^3$ with 5 different conductivities $\sigma = 10^6, 10^4, 10^3, 100$ and 50 at time $T = 90$. The ACM66 solution converges for the viscous resistive model for $\sigma = 10^6, 10^5, 10^3, 100$ and 50 using grid sizes 1601×1601, 1601×1601, 801×801, 201×201 and 201×201, respectively. For ideal MHD, the fine scale structures are quite well resolved using a 1601×1601 grid. However, grid convergence has not been obtained for this case. Comparing Figs. 6 and 7, one can see that lower accuracy and diffusive shock-capturing schemes such as MUSCL for the ideal MHD is similar to that of the solution of added $Re = 1000$ and $\sigma = 10^3$ by ACM66. See Fig. 6(c) and Fig. 7(d). The resolution of WENO5 and Harten-Yee TVD schemes exhibit a similar diffusive pattern as MUSCL.

Figure 8 shows the comparison of viscous resistive MHD for $Re = 10^8$ with 6 conductivity coefficients

Vortex Pairing in a Time-Developing Mixing Layer

(M_c=0.8, Re=1000, T_R=300K, Prandtl #=0.72)

Normalized with vorticity thickness:

$$\delta_\omega = \frac{u_1 - u_2}{(du/dy)_{max}}$$

T & c: determined by assuming constant stagnation enthalpy

IC:

u_1=1, u_2=-1, T_1=T_2,

Inital shear profile: u = 0.5 tanh (2y)

Crocco-Busemann:

$$c^2 = c_1^2 + \frac{\gamma - 1}{2}(u_1^2 - u^2)$$

Initial perturbations:

$$v' = \sum_{k=1}^{2} a_k \cos(2\pi k x / L_x + \phi_k) e^{(-y^2/b)} \qquad L_x = 30, b = 10$$

$$a_2 = 0.05, \phi_2 = -\pi/2$$

$$a_1 = 0.01, \phi_1 = -\pi/2$$

BC: Periodic in x, slip walls in y

Grids:

$$y = \frac{L_y}{2}\frac{\sinh(b_y \eta)}{\sinh(b_y)}, \quad L_y = 100,\ b_y = 3.4$$

uniform in x

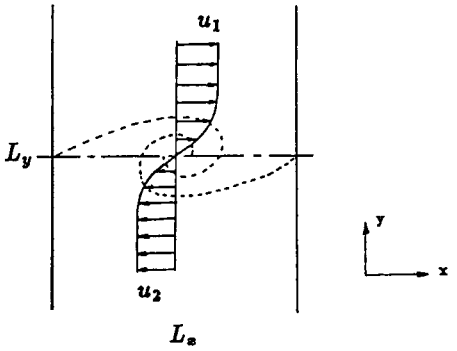

Fig. 5. Vortex pairing in time-developing mixing layer gas dynamics problem.

$\sigma = 10^6, 10^4, 10^3, 100, 50$ and 10 at $T = 90$. The ACM66 solution converges for $\sigma = 10^3, 100$ and 50 using a grid of 1601×1601, 801×801 and 401×401, respectively. For the three higher $\sigma = 10^6, 10^5, 10^3$, the fine scale structures are quite well resolved using a 1601×1601 grid. However, grid convergence has not been obtained for these three σ values on the very fine scale structures of the flow.

The study in[23] gives some insights on the effect of the resistive and viscous terms compared with ideal MHD. The most interesting result is that without adaptive numerical dissipation control, the commonly used shock-capturing schemes such as MUSCL, TVD and WENO5 solving the ideal MHD produce solutions as if added physical dissipation were present.

With the Hall term included, for small Hall coefficient $\beta_h < 0.2$ there is not much effect on the overall flow structure over the pure resistive MHD with the same Re and plasma β_p. As the Hall coefficient is increased beyond 0.2, the problem becomes more stiff and the computation using our filter scheme is stable only with grids that are smaller than 801×801. Although the more diffusive MUSCL and Harten-Yee are stable for a denser grid, the resolution is similar to the coarser grid solution by the filter method. Figure 9 shows three computations with different Hall coefficient β_h and conductivity coefficient σ. With the studied flow parameters, the Hall MHD flow patterns deviate from the resistive MHD slightly. For larger β_h, all considered methods become unstable even with smaller Re and σ values.

Concluding Remark: Our preliminary study on the two test cases shows the effect of the resistive and Hall coefficients on the flow structures compared with the ideal MHD. The result of the two blunt body problems indicate plasma injection can alter the shock standoff distance and heating. The study also sheds some light on a simplified model related to solar wind physics. Both test cases indicate that the Hall term with large Hall coefficient poses a challenge in numerical modeling and simulation. Additional investigation is planned to overcome the numerical instability for large Hall coefficients.

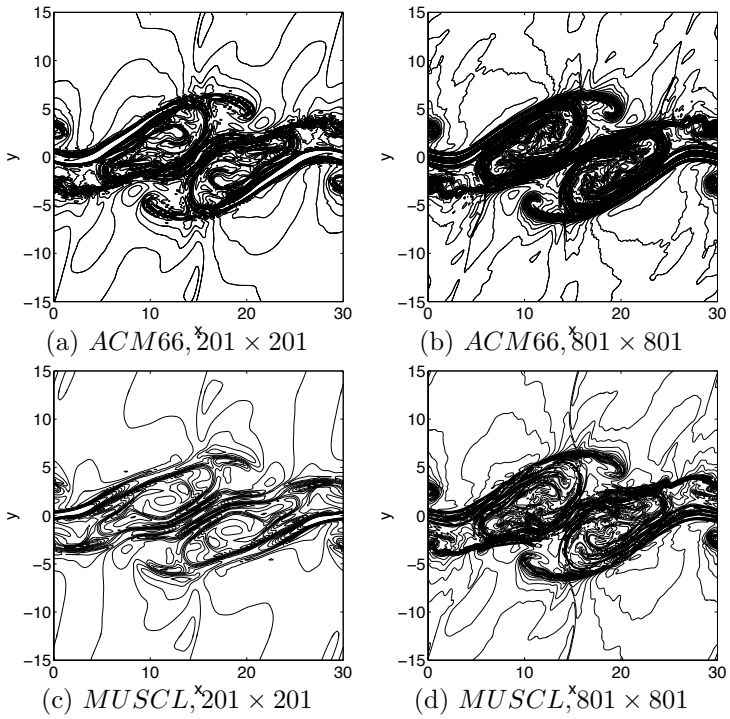

Fig. 6. Comparison of the temperature contours of ACM66 (top row) with MUSCL (bottom row) at $T = 90$ *for ideal MHD using* 201×201 *and* 801×801 *grids.*

References

[1]A. Bhattacharjee, *Impulsive Magnetic Reconnection in the Earth's Magnetotail and the Solar Corona*, Annu. Rev. Astron. Astrophys. **42**, 365 (2004).

[2]Q.-L. Fan, X.-S. Feng and C.-Q. Xiang, *Magnetohydrodynamics of Turbulent Magnetic Reconnection*, Physics of Plasma, **11**(12), 5605 (2004).

[3]D.V. Gaitonde, *Development of a Solver for 3-D Non-Ideal Magnetogasdynamics*, AIAA Paper 99-3610, 1999.

[4]K. Galsgaard, F. Moreno-Insertis, V. Archontis and A. Hood, *A Three-Dimensional Study of Reconnection, Current Sheets, and Jets Resulting From Magnetic Flux Emergence in the Sun*, Astrophysical J., **618**, 153 (2005).

[5]S.K. Godunov *Symmetric Form of the Equations of Magnetohydrodynamics,* Numerical Methods for Mechanics of Continuum Medium, **13** (1), 26 (1972).

[6]D. Grasso et al. Phys. Rev. Lett, **86**, 5051 (2001).

[7]M. Hesse and M. Kuznetsova, *The Role of Electron Heat Flux in Guide Field Magnetic Reconnection*, Physics of Plasma, **11**(12), 5387 (2004).

[8]J.D. Huba *Hall Magnetic Reconnection: Guide Field Dependence*, Physics of Plasma, **12**, 012322 (2005).

[9]A. Lazarian *3-D Reconnection in the Presence of Turbulence*, 2004.

[10]N.V. Pogorelov Nonevolutionary MHD Shocks. : A Critical Survey, Proceedings of the HYP2004, September 13-16, 2004.

[11]D. Del Sarto et al. Phys. Rev. Lett, **91**, 235001 (2003).

[12]B. Sjögreen and H. C. Yee, *Multiresolution Wavelet Based Adaptive Numerical Dissipation Control for Shock-Turbulence Computation*, RIACS Technical Report TR01.01, NASA Ames research center (Oct 2000); also, J. Scient. Computing, **20**, 211 (2004).

[13]B. Sjögreen and H.C. Yee, *Efficient Low Dissipative High Order Schemes for Multiscale MHD Flows, I: Basic Theory*, AIAA 2003-4118, Proceedings of the 16th AIAA/CFD Conference, June 23-26, 2003, Orlando, Fl.

[14]H. De Sterck and S. Poedts, *Field-aligned Magnetohydrodynamic Bow Shock Flows in the Switch-on Regime*, Astron. Astrophys. **343**, 641 (1999).

[15]M. Vinokur and H.C. Yee *Extension of Efficient Low Dissipative High Order Schemes for 3-D Curvilinear Moving Grids,* NASA TM 209598, June 2000; also, Frontiers of Computational Fluid Dynamics, 2002, World Scientific, D.A. Caughey & M. Hafez editors., pp. 129-164 (2002).

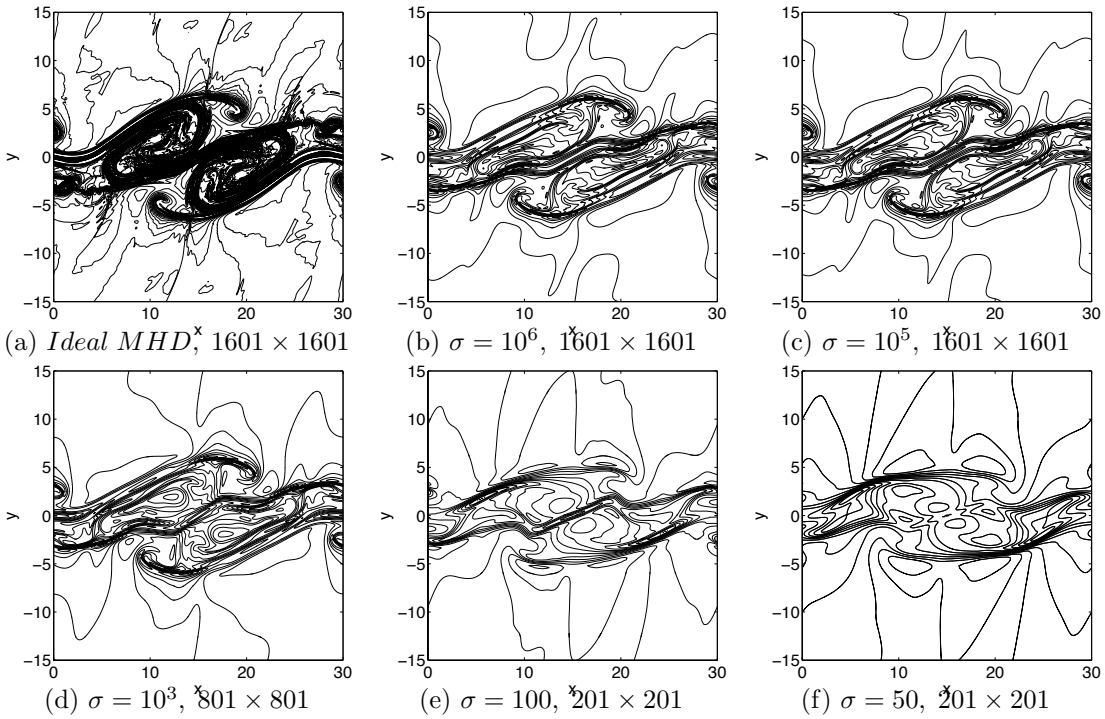

Fig. 7. Temperature contours of ACM66 for ideal and non-ideal MHD (Re = 1000, conductivities $\sigma = 10^6, 10^5, 10^3, 100, 50$*) at* $T = 90$.

[16]H.C. Yee, *A Class of High-Resolution Explicit and Implicit Shock-Capturing Methods*, VKI Lecture Series 1989-04, March 6-10, 1989, also NASA TM-101088, Feb. 1989.

[17]H.C. Yee, N.D. Sandham, N.D., and M.J. Djomehri, *Low Dissipative High Order Shock-Capturing Methods Using Characteristic-Based Filters*, J. Comput. Phys., **150**, 199 (1999).

[18]H.C. Yee and B. Sjögreen, *Designing Adaptive Low Dissipative High Order Schemes for Long-Time Integrations*, **Turbulent Flow Computation**, (Eds. D. Drikakis & B. Geurts), Kluwer Academic Publisher (2002); also RIACS Technical Report TR01-28, Dec. 2001.

[19]H.C. Yee *Building Blocks for Reliable Complex Nonlinear Numerical Simulations*, **Turbulent Flow Computation**, (Eds. D. Drikakis & B. Geurts), Kluwer Academic Publisher (2002).

[20]H.C. Yee and B. Sjögreen, *Divergence Free High Order Filter Methods for the Compressible MHD Equations,* Proceedings of the International Conference on High Performance Scientific Computing, March 10-14, 2003, Hanoi, Vietnam.

[21]H.C. Yee and B. Sjögreen, *Efficient Low Dissipative High Order Scheme for Multiscale MHD Flows, II: Minimization of Div(B) Numerical Error*, RIACS Technical Report TR03.10, July 2003, NASA Ames Research Center, to appear, J. Scient. Computing (2005).

[22]H.C. Yee and B. Sjögreen, *Nonlinear Filtering and Limiting in High Order Methods for Ideal and Non-Ideal MHD*, Proceedings of the ICOSAHOM-04, June 21-25, 2004, Brown University, Providence, RI; to appear, J. Scient. Computing (2005).

[23]H.C. Yee and B. Sjögreen, *Performance of Adaptive Numerical Dissipation Control in High Order Methods for the Resistive MHD Equations*, Proceedings of the HYP2004, Sept. 13-17, 2004, Osaka, Japan.

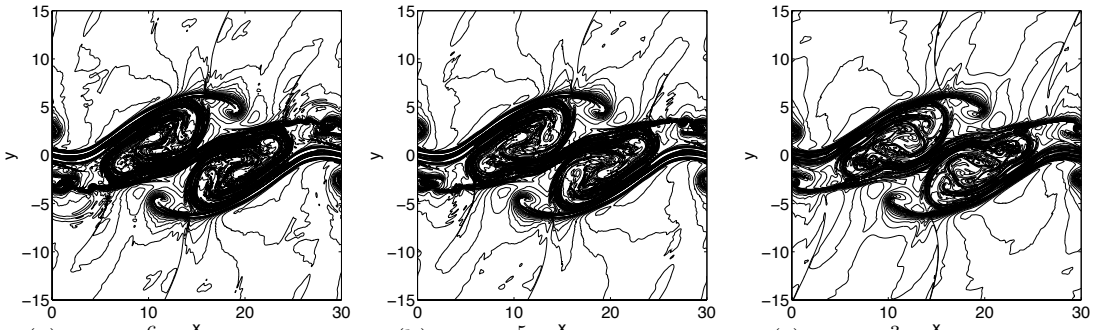

(a) $\sigma = 10^6,\ 1601 \times 1601$ (b) $\sigma = 10^5,\ 1601 \times 1601$ (c) $\sigma = 10^3,\ 1601 \times 1601$

(d) $\sigma = 100,\ 1601 \times 1601$ (e) $\sigma = 50,\ 1601 \times 1601$ (f) $\sigma = 10,\ 401 \times 401$

Fig. 8. Temperature contours of ACM66 for non-ideal MHD with $Re = 10^8$ *and conductivities* $\sigma = 10^6, 10^5, 10^3, 100, 50, 10$ *at* $T = 90$.

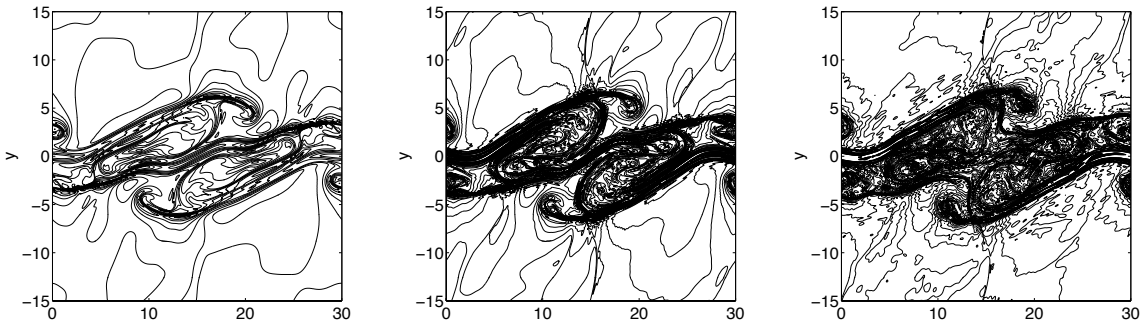

(a) $\sigma = 10^3,\ \beta_h = 0.1,\ Re = 10^5$ (b) $\sigma = 10^5,\ \beta_h = 0.2,\ Re = 10^5$ (c) $\sigma = 10^5,\ \beta_h = 0.5,\ Re = 10^5$

Fig. 9. Temperature contours of ACM66 for three β_h *for non-ideal MHD with* $Re = 10^5$ *and conductivities* $\sigma = 10^3, 10^5$ *using a* 801×801 *grid at* $T = 90$.